Anomalous ferroelectricity and double-negative effects in bilayer hexagonal boron nitride

Wen Jiang,[1,2] Chang Liu,[1,2] Xiaonan Ma,[1,2] Xing Yu,[1,2] Shunbo Hu,[1,2,*] Xi Li,[1,2] Lee A. Burton,[1] Yu Liu,[1,2] Yangyang Chen,[1,2,†] Pan Guo,[1,2] Xiangyang Kong,[3] Laurent Bellaiche,[4] and Wei Ren[1,2,‡]

[1]*Physics Department, Materials Genome Institute, Shanghai Key Laboratory of High Temperature Superconductors, State Key Laboratory of Advanced Special Steel, International Centre of Quantum and Molecular Structures, Shanghai University, Shanghai 200444, China*

[2]*Zhejiang Laboratory, Hangzhou 311100, China*

[3]*Institute of Materials for Mobile Energy, School of Materials Science and Engineering, Shanghai Jiao Tong University, Shanghai 200240, China*

[4]*Physics Department, Institute for Nanoscience and Engineering, University of Arkansas, Fayetteville, Arkansas 72701, USA*

(Received 1 February 2022; revised 15 July 2022; accepted 15 July 2022; published 15 August 2022)

Recently, the presence of an out-of-plane ferroelectric polarization was experimentally confirmed in bilayer two-dimensional (2D) hexagonal boron nitride (h-BN). In this work, we employ first-principles computations to reveal that (i) such slidetronic ferroelectricity is electronic in nature and arises from in-plane interlayer translation, which is distinctive among 2D slidetronic ferroelectric materials; and (ii) there is a coexistence of a negative longitudinal piezoelectric effect and an out-of-plane negative Poisson's ratio in the ferroelectric state of bilayer h-BN, which we refer to as anomalous double-negative effects.

DOI: 10.1103/PhysRevB.106.054104

I. INTRODUCTION

Traditional ferroelectric materials are facing the challenge of continuous miniaturization for integrated electronic components. Two-dimensional (2D) structures can be employed in a wide range of applications, including flexible electronics, strain sensors, nanogenerators, and innovative nanoelectromechanical systems. The ultrasmall thickness of atomic layers in 2D ferroelectrics may enable higher data storage densities, and the van der Waals (vdW) interactions at 2D interfaces allow for high-quality lattice interfaces in the epitaxial growth. Therefore, numerous studies have focused on the exploration of 2D vdW ferroelectric materials in recent years [1–6]. Theoretically, Shirodkar and Waghmare [7] predicted an out-of-plane spontaneous polarization in the 1T-MoS_2 monolayer. Large in-plane ferroelectric polarization and high Curie temperatures were also found in monolayer γ-SbX (X = As, P) [8]. Interestingly, under certain conditions, the coupled in-plane and out-of-plane ferroelectric polarizations can coexist in some vdW multilayer materials [9]. For example, ferroelectricity was also proposed in 2D phosphorus oxide P_2O_3, with polarization both perpendicular and parallel to the lateral plane [10]. Experimentally, the research progress of 2D vdW ferroelectric materials is also rapidly developing, and the recent successful preparation of a variety of 2D vdW ferroelectric materials has greatly motivated researchers to explore new applications for functional devices [11–14].

Due to its remarkable physical properties and wide application potential, graphene has been the focus of various frontiers in 2D vdW materials over the past decade. In 2004, Novoselov *et al.* [15] first used tape to strip graphene from graphite, and built an electronic device to measure its unique quantum Hall effect. It is well known that 2D hexagonal boron nitride (h-BN) and graphene are very similar in terms of the honeycomb lattice structure [16], and monolayer h-BN also has an atomically smooth surface and is known as white graphene [17]. The band gap of graphene is 0 eV when the spin-orbit coupling is absent, and this disadvantage has limited its possible transistor applications. Compared to graphene, 2D h-BN is a wide-band gap insulator [18,19]. Moreover, previous works have shown that 2D h-BN is an ideal substrate for growing 2D materials with great flexibility, which plays an increasingly important role in semiconductor device design [19,20]. Over the past few years, many different experimental methods have been developed to study 2D monolayer or multilayer h-BN. For example, molecular beam epitaxy is considered an effective way to control the growth of 2D multilayer h-BN on a transition metal surface [21], and low-pressure chemical vapor deposition also allows the synthesis of h-BN with a controlled number of layers [22]. Very recently, Yasuda *et al.* [23] and Vizner Stern *et al.* [24] formed polar bilayer h-BN devices by using the "tear and stack" method, and bistable out-of-plane ferroelectric polarization was successfully measured in their experimental reports.

Piezoelectricity is the ability of a noncentrosymmetric material to generate polarized charge in response to externally applied mechanical stress. In recent years, the search for piezoelectric materials and attempts to uncover their unique electronic properties have been keenly pursued by the 2D research community. In low-dimensional systems, the negative piezoelectric properties are rarely considered with negative longitudinal piezoelectric coefficients (e_{33} and d_{33}), where the polarization in the material increases under a vertical pressure

*shunbohu@shu.edu.cn
†phycyy@shu.edu.cn
‡renwei@shu.edu.cn

along the polarization direction. For instance, negative piezoelectricity in low-dimensional materials was investigated by Qi and Rappe [25] using $CuInP_2S_6$ as an example. They concluded that the negative piezoelectricity of $CuInP_2S_6$ arises from a negative clamped-ion and a near-zero internal strain term [25]. Moreover, in order to investigate more fully the mechanical properties of 2D materials, Poisson's ratio is also taken into consideration as a fundamental mechanical parameter [26]. It describes the response of a material to externally applied uniaxial stress, which was first proposed by the French mathematician and physicist Poisson. Poisson's ratio is positive in most materials, yet negative Poisson's ratio materials have attracted great interest due to their possible applications in aerospace and medical applications. For instance, Jiang *et al.* [27,28] calculated the existence of an out-of-plane negative Poisson's ratio in monolayer black phosphorus by using first principles, which was subsequently confirmed experimentally.

In the present work, we comprehensively study different stacking orders of 2D bilayer h-BN using two different theoretical approaches to verify the out-of-plane ferroelectric polarization. The results are strongly consistent with available experimental data of 2D bilayer h-BN. In addition, the microscopic mechanism and strain engineering of physical properties are further explained. When the interlayer spacing and in-plane lattice constants are considered for ferroelectric and mechanical properties, we predict an interesting coexistence of a negative longitudinal piezoelectric effect and an out-of-plane negative Poisson's ratio in the ferroelectric state of bilayer h-BN.

II. METHODS

We use here first-principles calculations based on the density functional theory (DFT), and employ the Vienna Ab initio Simulation Package (VASP) [29,30] to predict geometric and electrical properties. The electron exchange and correlation functionals were treated by the generalized gradient approximation of Perdew–Burke–Ernzerhof (PBE) [31]. Moreover, local density approximation (LDA) [32] and Perdew-Burke-Ernzerhof revised for solids (PBEsol) [33] were used for the sake of comparison for properties of bulk and bilayer h-BN. The importance of van der Waals interactions is also considered in this work, using PBE-D2 and PBE-optB86b correlation functionals. Furthermore, and in order to achieve higher accuracy, we also chose the HSE06 method developed by Heyd *et al.* [34] and the GW_0 [35] method to investigate electronic band gaps further. The lattice constants and ions are relaxed until the residual force on each atom falls below 0.001 eV $Å^{-1}$, and the convergence criterion for the total energy calculations is set as 10^{-9} eV. Γ-centered k-grids are adopted with the smallest allowed spacing: ∼0.03 $Å^{-1}$. We also used the Gaussian smearing method with a width of 0.05 eV. The Berry phase theory [36,37] and the Wannier charge center method [38] were used to compute the electrical polarization. In order to avoid spurious interactions between the periodic images, we set the vacuum space to be 25 Å. To prove the stability of the structure, phonon spectra are evaluated by VASP together with the PHONOPY program, and the $2 \times 2 \times 1$ supercell is generated for the phonon calculations [39–41]. Additionally, *ab initio* molecular dynamic (AIMD) [42] simulation is carried out in a microcanonical ensemble, with a time step of 3.0 fs and a total simulation time of 3.0 ps.

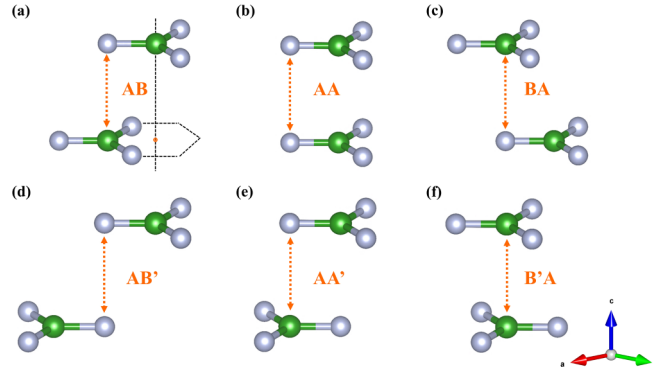

FIG. 1. Six different stacking orders of bilayer h-BN. (a)–(c) are (B–N bonds) parallel configurations and (d)–(f) are antiparallel configurations. The green and silver spheres represent B and N atoms, respectively.

III. RESULTS AND DISCUSSION

The crystal space group of the ground-state bulk h-BN is $P6_3/mmc$ [43], in which the B atoms in the upper layer are located on top of the N atoms in the lower layer, and the N atoms in the upper layer sit directly above the B atoms of the lower layer (see AA′ in Fig. 1). As shown in Supplemental Material Table S1 [44], when the bulk h-BN is optimized using the PBEsol functional, the calculated lattice constants are very close to the experimental values [45]. Moreover, monolayer h-BN can be obtained from h-BN crystals using mechanical exfoliation techniques as accomplished in graphene [46]. For bilayer h-BN, there are more possible stacking arrangements than for bilayer graphene.

We construct bilayer h-BN with six different stacking orders, as shown in Fig. 1. The structure shown in Fig. 1(b) is known as the AA stacking order and is made of two identical h-BN layers attached to each other. We can fix one layer of the structure in Fig. 1(b) and slide the other layer (along a B—N bond-length direction) to obtain the two structures displayed in Figs. 1(a) and 1(c), which are dubbed the AB and BA stacking orders, respectively. If we focus on the AB stacking, the bottom-layer B atom aligns in the same vertical line as the top-layer N atom, whereas the top-layer B atom is located above the center of hexagon underneath. The illustration shown in Fig. 1(e) is the AA′ stacking order, with all B—N bonds in two layers being antiparallel to each other (and all B—N bonds in two layers are parallel in the AA stacking). Similarly, Figs. 1(d) and 1(f) are obtained by sliding the AA′ stacking layer (along the B—N bond-length direction) to generate AB′ and B′A stacking orders. We calculate structural parameters, point groups, and relative energies for all six stacking orders, with the results shown in Table I. The AB and BA stacking orders are at the relative position of the energy minimum.

The ferroelectric polarization is formed in the AB and BA stacking orders, along the out-of-plane direction, reversible between the AB and BA switching (via relative interlayer slide along the in-plane direction between two layers). As a

TABLE I. Structural parameters, point groups and relative energies of the six stacking orders of bilayer h-BN by using the PBE-D2 correction method of Grimme.

Stacking order	AA	AB (BA)	AA′	AB′	B′A
Lattice parameter (Å)	2.502	2.502	2.502	2.502	2.501
Interlayer spacing (Å)	3.402	3.077	3.110	3.356	3.130
Point group	$\bar{6}$m	3m	$\bar{3}$m	$\bar{3}$m	$\bar{3}$m
ΔE (meV/unit cell)	46.430	0	3.226	42.304	10.091

result, the AB and BA stacking orders are referred to as the ferroelectric bistable states. Note that, recently, two independent experiments have been reported in which the AB and BA possess spontaneous ferroelectric polarization [23,24]. One team detected the ferroelectric polarization switching evidence through the resistance of an adjacently stacked graphene sheet to the bilayer h-BN [23]. Meanwhile, the other team directly observed that alternating domains of inverted normal polarization in AB and BA stacking orders were separated by sharp domain walls [24]. Here, we discuss the polarization of the AB stack order using first-principles calculations from an atomistic point of view. Table II shows that the various functionals and vdW corrections might have a significant effect on the structural properties of bilayer h-BN. As a matter of fact, they modify substantially the interlayer spacing, resulting in a large variation of the polarization.

Particularly, after optimizing the in-plane lattice constants and atomic positions by using the PBE-D2 correction method of Grimme [47], the ferroelectric polarization of such bilayer h-BN is about 2.00 pC m^{-1} from our Berry phase calculation. The ferroelectric polarization of the AB stacking is in the positive direction along the c-axis, whereas that of the BA stacking is in the negative direction. We also employ the Wannier charge center method and obtain a ferroelectric polarization of about 2.14 pC m^{-1}, to be compared with the measurement value of 2.25 pC m^{-1} obtained at $T = 4.2$ K [23]. Therefore, our computational results agree well with the measurements, and are also close to previous theoretical calculation reports [1,23,24,48]. It is assumed in the literature that ferroelectricity is usually derived from ionic displacements, while in conventional perovskite ferroelectric materials such as barium titanium oxide ($BaTiO_3$), ferroelectricity generally originates from both ionic and electronic contributions. Interestingly, the

TABLE II. Lattice parameter, interlayer spacing, ferroelectric polarization, and energy barrier of the AB stacking order, as predicted by using different functionals.

Functional	Lattice parameter (Å)	Interlayer spacing (Å)	Polarization (pC m^{-1})	Energy barrier (meV/unit cell)
PBE-D2	2.502	3.077	2.00	8.56
LDA	2.482	3.208	1.42	5.11
PBE-optB86b	2.502	3.252	1.31	4.56
PBEsol	2.497	3.514	0.63	1.97
PBE	2.504	4.256	0.08	0.21
Experiment [23]			2.25	

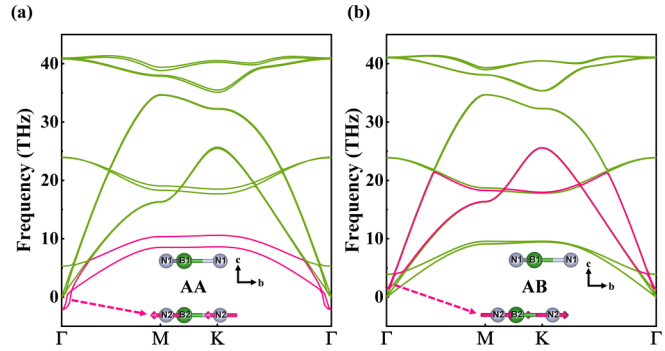

FIG. 2. Phonon spectra of bilayer h-BN in the (a) paraelectric state and (b) ferroelectric state. The pink dashed arrows highlight the subtle sign difference of phonon frequencies at the Γ point.

out-of-plane ferroelectric polarization of bilayer h-BN solely arises from the contribution of electrons in the Berry phase calculation, which is very similar to the electron polarization of type II multiferroics [49–60]. However, the symmetry breaking here is due to the bilayer sliding. As shown in Fig. 2(a), we also calculated the phonon dispersion of the AA paraelectric phase, and find that there are two degenerate imaginary frequencies at the Γ point of the Brillouin zone. Such imaginary frequencies correspond to the soft optical modes (Γ_3), representing slide modes of bilayer h-BN. Upon interlayer sliding, these modes become positive in frequency and then one can obtain stable AB stacking of a ferroelectric structure, as shown in Fig. 2(b). It is worth noting that such sliding displacement does not induce any ionic polarization along the c direction. According to the previous discussions, we believe the normal polarization comes from interlayer coupling in company with a sliding-induced symmetry breaking.

Figure 3 shows the top and side views of the differential charge density isosurface of bilayer h-BN in three states (AB, AA, and BA). The yellow and purple areas indicate the regions that gained and lost electrons, respectively. It is evident that the atomic environment of the bottom and top atoms in the AB or BA bilayer h-BN is locally nonsymmetric, and charge transfer occurs between two layers. Moreover, the electron gain and loss regions between the ferroelectric bistable AB and BA states are exchanged, which is consistent with the reversal of the direction of their ferroelectric polarization. For the unstable AA state, the isosurface is symmetric for the paraelectric configuration along the out-of-plane direction. Furthermore, we run AIMD simulations to evaluate the thermal stability of AB at the temperature of 300 K, as shown in Supplemental Material Fig. S1 [44]. The calculated elastic constants are provided in Supplemental Material Table S2 [44], which also satisfy the Born criterion for 2D hexagonal structures [61,62].

Using the climbing image nudged elastic band calculations, we find that ferroelectric switching should overcome an energy barrier of about 8.56 meV/unit cell, as shown in Fig. 4, which displays the path connecting the ferroelectric bistable states via the intermediate state of bilayer h-BN. This energy barrier makes the switching between two ferroelectric states much easier than through the paraelectric AA state. The switching between the AB and BA states could be quantified

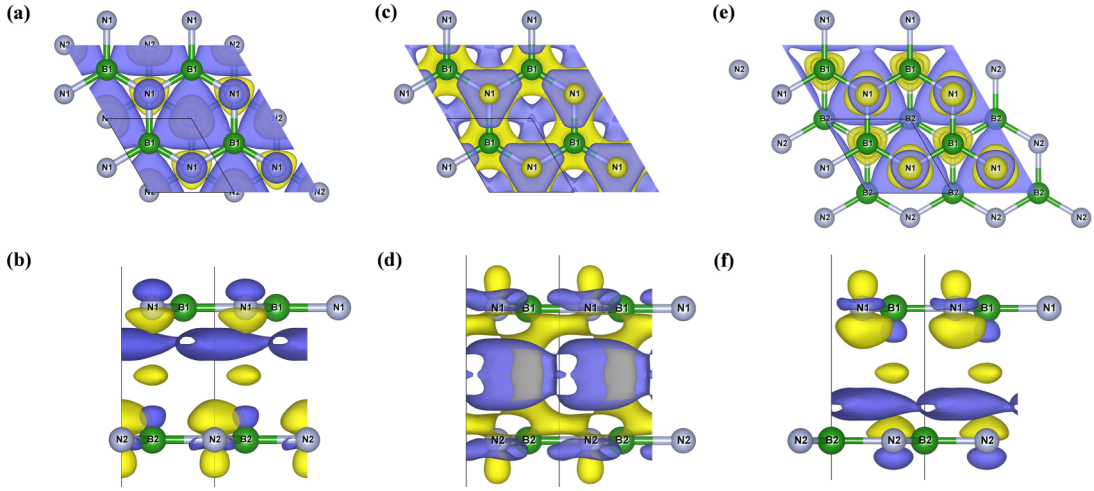

FIG. 3. The top and side views of the differential charge density diagrams of the (a) and (b) AB stacking, (c) and (d) AA stacking, and (e) and (f) BA stacking bilayer h-BN.

as the in-plane displacement along the $[1\bar{1}0]$ direction when the upper layer B and N atoms are fixed. The magnitude of such translation is one B—N bond length of approximately 1.44 Å. We confirm that the energy of ferroelectric bistable states is not the local minimum, but rather the ground state.

According to many theoretical and experimental works, low-dimensional materials are known to respond effectively to external stimuli [63,64]. Here, we investigate how the ferroelectricity and elasticity vary when the interlayer spacing and in-plane lattice constants change. Since the ferroelectric polarization in the AB stacking order is along the out-of-plane direction, we first discuss the effect of the interlayer spacing change on the polarization. Surprisingly, it is found that the ferroelectric polarization is inversely proportional to the interlayer spacing—i.e., the polarization increases when compressing the interlayer spacing, but decreases upon expanding the interlayer spacing. As shown in Fig. 5(a), the out-of-plane ferroelectric polarization of the system gradually goes to zero when the interlayer distance is greater than 4.5 Å, while it is dramatically enhanced when the interlayer distance is suppressed from 3.5 Å to 2.5 Å. This is similar to three-dimensional negative piezoelectric materials, such as hexagonal ABC ferroelectrics (KMgSb, NaZnSb, etc.)

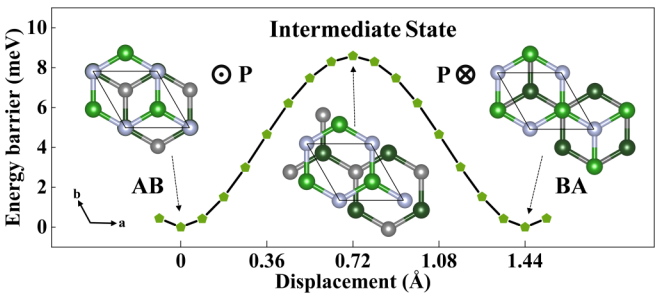

FIG. 4. The ferroelectric switching path along the $[1\bar{1}0]$ direction and the energy barrier of bilayer h-BN from the bistable AB to BA configuration. Dark colors indicate the bottom-layer atoms of bilayer h-BN. The two lowest energy points in the double-well potential curve correspond to the bistable AB and BA states.

[65] and BiTeX (X = Cl, Br, I) [66]. The variation of the in-plane lattice constant with different interlayer distances is almost negligible when the structural relaxation is allowed. The enhancement of polarization is thus mainly due to the increase of electric dipole moments. The Hirshfeld-I charges of the B and N atoms at different interlayer spacing are listed in Supplemental Material Table S3 [44,67]. Using our calculated elastic constants C_{ij}, the relation between piezoelectric coefficients e_{ij} and d_{ij} can be expressed as

$$e_{ij} = \sum_{k=1}^{6} d_{ik} C_{kj}, \tag{1}$$

with i, j, $k = 1, 2, 3$, corresponding to the a, b, and c axes, respectively. Considering that the AB stacking order belongs to the 3m point group, we obtain the relationship among the piezoelectric stress tensors e_{ij}, piezoelectric strain tensors d_{ij}, and elastic tensors C_{ij}:

$$\begin{pmatrix} 0 & 0 & 0 & 0 & e_{15} & -e_{22} \\ -e_{22} & e_{22} & 0 & e_{15} & 0 & 0 \\ e_{31} & e_{31} & e_{33} & 0 & 0 & 0 \end{pmatrix} = \begin{pmatrix} 0 & 0 & 0 & 0 & d_{15} & -d_{22} \\ -d_{22} & d_{22} & 0 & d_{15} & 0 & 0 \\ d_{31} & d_{31} & d_{33} & 0 & 0 & 0 \end{pmatrix} \times \begin{pmatrix} C_{11} & C_{12} & C_{13} & C_{14} & 0 & 0 \\ C_{12} & C_{11} & C_{13} & -C_{14} & 0 & 0 \\ C_{13} & C_{13} & C_{33} & 0 & 0 & 0 \\ C_{14} & -C_{14} & 0 & C_{44} & 0 & 0 \\ 0 & 0 & 0 & 0 & C_{44} & C_{14} \\ 0 & 0 & 0 & 0 & C_{14} & 0.5(C_{11} - C_{12}) \end{pmatrix} \tag{2}$$

The piezoelectric coefficient is calculated to be $d_{33} = -0.97$ pm/V, which exhibits the negative longitudinal piezoelectricity. The e_{33} is commonly decomposed into a "clamped ion" contribution ($e_{33,c}$) and an "internal strain" contribution ($e_{33,i}$) [68]. The former describes the change of polarization

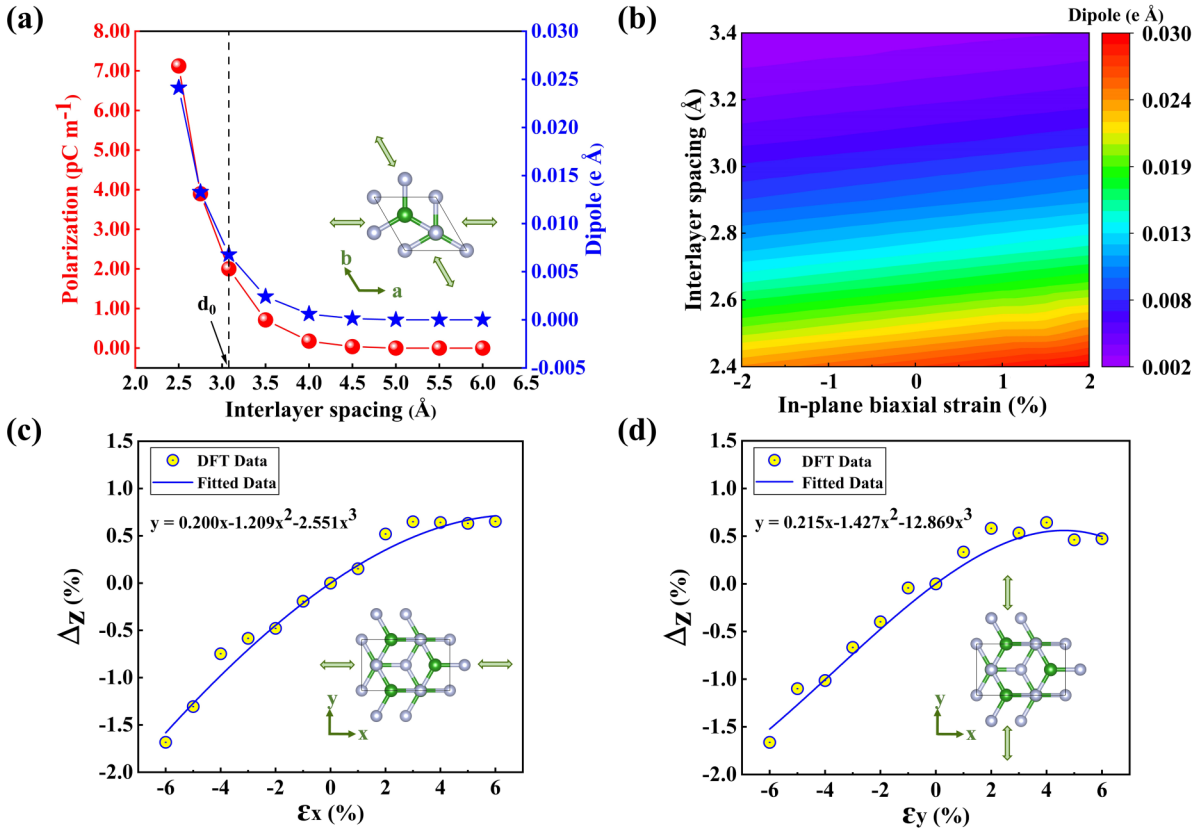

FIG. 5. (a) Interlayer spacing effect on the ferroelectric polarization and electric dipole moment. (b) Interlayer spacing and in-plane biaxial strain phase diagram of the electric dipole moment. The change of out-of-plane direction interlayer distance (Δ_z) versus strain along the (c) x direction and (d) y direction. Note we use a hexagonal lattice in (a) and (b), and an orthorhombic lattice in (c) and (d). The lattice constants between them are related as $a_h = \frac{1}{\sqrt{3}}x_o$ and $b_h = y_o$.

due to a uniform distortion of the lattice, while the latter measures the piezoelectric response to atomic relaxations that release the internal strain. Our negative longitudinal piezoelectric effect is caused by the negative internal strain contribution in the AB configuration. It does not exist in other stacking orders of bilayer h-BN; i.e., the piezoelectricity is not present in the AA′, AB′, and B′A stacking orders, while the positive piezoelectric coefficient is $d_{22} = 0.58$ pm/V in the AA configuration. In Fig. 5(b), the combined effects of interlayer spacing and in-plane biaxial strain (from -2% to 2%) on the electric dipole moment are shown in a phase diagram. The in-plane biaxial strain used here is defined as $\varepsilon = (a - a_0)/a_0 \times 100\%$, where a and a_0 are the lattice constants with and without applied strain, respectively. When the in-plane tensile strain increases while the interlayer spacing is compressed, the electric dipole moment is found to increase. Therefore, the ferroelectricity can be effectively tuned by changing the structure's parameters. The in-plane biaxial strain effects on other physical properties are shown in Supplemental Material Table S4 [44]. Interestingly, upon relaxation, the interlayer spacing increases with the increasing in-plane tensile strain, which suggests a completely opposite trend compared to other reported bilayer materials—e.g., bilayer WTe_2 [4]. Moreover, we further extend the range of uniaxial strain from -6% to 6% and demonstrate that this is an auxetic effect, meaning an increase in volume under tension and a decrease in volume under compression. The changes of out-of-plane direction (Δ_z) versus strain along the strain of the x direction and y direction are shown in Figs. 5(c) and 5(d). The data are fitted to a polynomial function $y = -\nu_1 x + \nu_2 x^2 + \nu_3 x^3$, and $\nu = \nu_1$ is the linear Poisson's ratio. Here, we calculate and estimate how the AB stacking order responds structurally to uniaxial strain in the x and y directions. The in-plane Poisson's ratio is positive when applying strain along the x and y directions. The fitted curves and the positive Poisson's ratio obtained are shown in Supplemental Material Fig. S2 [44]. The negative Poisson's ratio (NPR) is not uncommon in 2D materials with hinge-like structures [27,69]. A previous work has also reported NPR for both AB bilayer graphene and AA′ bilayer h-BN along the out-of-plane direction [70]. Due to the similar honeycomb structure, it is expected that an auxetic effect may also exist in the AB stacking order of bilayer h-BN.

Remarkably, the out-of-plane NPR is -0.200 when the strain is along the x direction, while reaching -0.215 when the strain is along the y direction, by fitting the data in Figs. 5(c) and 5(d). These two values are greater in magnitude than the NPR of all previous materials mentioned earlier. The B—N bond length and B—N—B bond angle gradually increase in response to a uniaxial strain, which is consistent with the NPR origin in two-dimensional honeycomb structures [71]. The extraordinary auxeticity renders the AB bilayer h-BN a

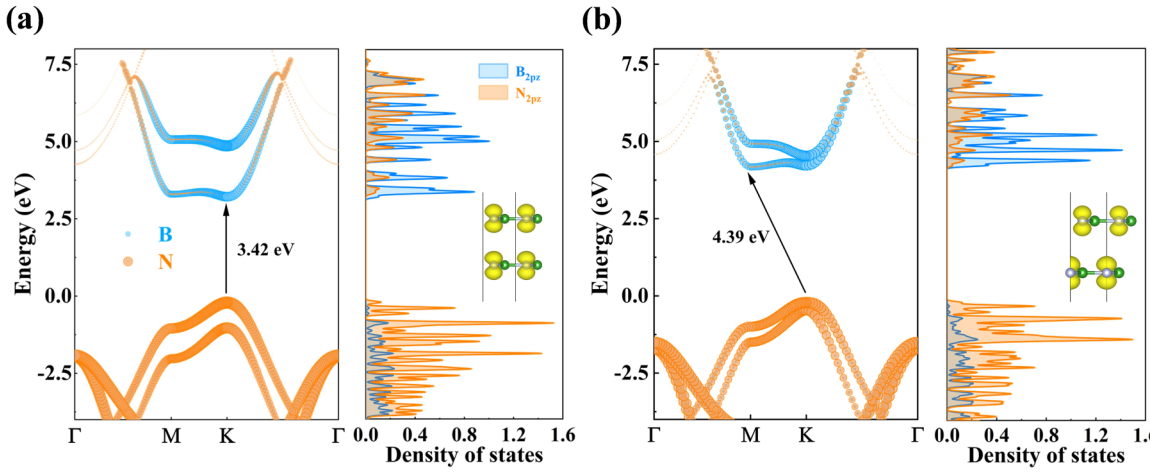

FIG. 6. The band structures and projected density of states of (a) the paraelectric AA bilayer h-BN and (b) the ferroelectric AB bilayer h-BN. The blue and orange colors indicate B and N states, respectively. The yellow areas in the insets represent the $2pz$ orbitals.

versatile candidate for improved toughness, shear resistance, or efficient sound/vibration absorption. We therefore reveal that the negative longitudinal piezoelectricity may coexist with the negative Poisson's ratio, as "anomalous double-negative effects," which are delicately related to the layered structures and stacking orders.

Ferroelectric bistable states with reversed ferroelectric polarization should also have identical electronic band structures. The band structure and the projected density of states of the paraelectric AA and the ferroelectric AB states are shown in Figs. 6(a) and 6(b), respectively. We can clearly see that the position of the conduction band minimum changes from the K point to the M point, and the direct band gap becomes indirect. The $2pz$ orbitals of the nitrogen are no longer overlapping, and the interorbital interaction is weakened, giving a larger band gap (by about 1 eV). Moreover, we calculate the band gap using three different exchange–correlation functionals and demonstrate that bilayer AB h-BN is a wide-band gap insulator with an indirect gap of 4.39 eV by PBE-D2. To avoid the well-known underestimation of the band gap, we further obtain an indirect band gap of 5.65 eV by employing hybrid functional HSE06, and an indirect band gap of 6.76 eV by GW_0 calculations. Under biaxial strain ranging from -2% to 2%, the indirect nature of the band gap of AB remains. Despite the fact that the band gap varies by only 0.24 eV due to the strain effect, we find that it depends linearly on the biaxial strain with a negative slope, as shown in Supplemental Material Fig. S3 [44].

IV. CONCLUSION

In summary, we perform comprehensive theoretical calculations and analyses of the structure, ferroelectric polarization, piezoelectricity, elastic (NPR) and electronic properties of bilayer h-BN. Of the six studied stacking orders of bilayer h-BN, the AB and BA configurations have a spontaneous out-of-plane ferroelectric polarization, and their polarization directions are opposite to each other. Bilayer h-BN is extremely simple in structure, and yet the ferroelectricity of it has only recently been confirmed experimentally. Our DFT calculations are not only in agreement with previous theoretical and experimental results, but also propose that the out-of-plane ferroelectricity of bilayer h-BN solely arises from the contribution of electrons. Moreover, in discussing the effect of interlayer spacing and in-plane strain on ferroelectricity and physical properties, we predict the coexistence of a negative longitudinal piezoelectricity and an out-of-plane negative Poisson's ratio in h-BN with the AB or BA stacking order. Such anomalous double-negative effects were never observed in conventional perovskite ferroelectrics, and we expect these extraordinary properties to be realized in fascinating 2D materials for advancing more valuable applications.

ACKNOWLEDGMENTS

This work was supported by the National Natural Science Foundation of China (Grants No. 12074241, No. 52130204, and No. 11929401); the Science and Technology Commission of Shanghai Municipality (Grants No. 19010500500, No. 20501130600, and No. 21JC1402700); the High Performance Computing Center, Shanghai University; and the Key Research Project of Zhejiang Laboratory (Grant No. 2021PE0AC02). L.B. thanks the Office of Naval Research (Grant No. N00014-21-1-2086) and the Vannevar Bush Faculty Fellowship (VBFF) Grant No. N00014-20-1-2834 from the Department of Defense.

[1] M. Wu and P. Jena, WIREs Comp. Mol. Sci. **8**, e1365 (2018).
[2] M. Wu, ACS Nano **15**, 9229 (2021).
[3] Y. Li, C. Liu, G.- D. Zhao, T. Hu, and W. Ren, Phys. Rev. B **104**, L060405 (2021).

[4] X. Liu, Y. Yang, T. Hu, G. Zhao, C. Chen, and W. Ren, Nanoscale **11**, 18575 (2019).

[5] X. Liu, A. P. Pyatakov, and W. Ren, Phys. Rev. Lett. **125**, 247601 (2020).

[6] Q. Yang, M. Wu, and J. Li, J. Phys. Chem. Lett. **9**, 7160 (2018).

[7] S. N. Shirodkar and U. V. Waghmare, Phys. Rev. Lett. **112**, 157601 (2014).

[8] S. Shen, C. Liu, Y. Ma, B. Huang, and Y. Dai, Nanoscale **11**, 11864 (2019).

[9] Y. Liang, S. Shen, B. Huang, Y. Dai, and Y. Ma, Mater. Horizons **8**, 1683 (2021).

[10] W. Luo and H. Xiang, Angewandte Chem. **55**, 8575 (2016).

[11] K. Chang, J. Liu, H. Lin, N. Wang, K. Zhao, A. Zhang, F. Jin, Y. Zhong, X. Hu, W. Duan, Q. Zhang, L. Fu, Q.- K. Xue, X. Chen, and S.- H. Ji, Science **353**, 274 (2016).

[12] M. Si, P.- Y. Liao, G. Qiu, Y. Duan, and P. D. Ye, ACS Nano **12**, 6700 (2018).

[13] S. Yuan, X. Luo, H. L. Chan, C. Xiao, Y. Dai, M. Xie, and J. Hao, Nat. Commun. **10**, 1775 (2019).

[14] Y. Zhou, D. Wu, Y. Zhu, Y. Cho, Q. He, X. Yang, K. Herrera, Z. Chu, Y. Han, M. C. Downer, H. Peng, and K. Lai, Nano Lett. **17**, 5508 (2017).

[15] K. S. Novoselov, A. K. Geim, S. V. Morozov, D. Jiang, Y. Zhang, S. V. Dubonos, I. V. Grigorieva, and A. A. Firsov, Science **306**, 666 (2004).

[16] C. Tarrio and S. E. Schnatterly, Phys. Rev. B **40**, 7852 (1989).

[17] L. Song, L. Ci, H. Lu, P. B. Sorokin, C. Jin, J. Ni, A. G. Kvashnin, D. G. Kvashnin, J. Lou, and B. I. Yakobson, Nano Lett. **10**, 3209 (2010).

[18] S. M. Kim, A. Hsu, M. H. Park, S. H. Chae, S. J. Yun, J. S. Lee, D.-H. Cho, W. Fang, C. Lee, T. Palacios, M. Dresselhaus, K. K. Kim, Y. H. Lee, and J. Kong, Nat. Commun. **6**, 8662 (2015).

[19] Y. Saito, M. Maida, and T. Matsumoto, Jpn. J. Appl. Phys. **38**, 159 (1999).

[20] W. Gao and A. Tkatchenko, Phys. Rev. Lett. **114**, 096101 (2015).

[21] A. A. Tonkikh, E. N. Voloshina, P. Werner, H. Blumtritt, B. Senkovskiy, G. Guentherodt, S. S. P. Parkin, and Y. S. Dedkov, Sci. Rep. **6**, 1 (2016).

[22] A. Ismach, H. Chou, D. A. Ferrer, Y. Wu, S. McDonnell, H. C. Floresca, A. Covacevich, C. Pope, R. Piner, and M. J. Kim, ACS Nano **6**, 6378 (2012).

[23] K. Yasuda, X. Wang, K. Watanabe, T. Taniguchi, and P. Jarillo-Herrero, Science **372**, 1458 (2021).

[24] M. Vizner Stern, Y. Waschitz, W. Cao, I. Nevo, K. Watanabe, T. Taniguchi, E. Sela, M. Urbakh, O. Hod, and M. Ben Shalom, Science **372**, 1462 (2021).

[25] Y. Qi and A. M. Rappe, Phys. Rev. Lett. **126**, 217601 (2021).

[26] C. Huang, W. Ren, V. C. Nguyen, Z. Chen, J. Wang, T. Sritharan, and L. Chen, Adv. Mater. **24**, 4170 (2012).

[27] J.-W. Jiang and H. S. Park, Nat. Commun. **5**, 4727 (2014).

[28] Y. Du, J. Maassen, W. Wu, Z. Luo, X. Xu, and P. D. Ye, Nano Lett. **16**, 6701 (2016).

[29] G. Kresse and J. Furthmuller, Phys. Rev. B **54**, 11169 (1996).

[30] G. Kresse and J. Furthmuller, Comput. Mater. Sci. **6**, 15 (1996).

[31] J. P. Perdew, K. Burke, and M. Ernzerhof, Phys. Rev. Lett. **77**, 3865 (1996).

[32] D. M. Ceperley and B. J. Alder, Phys. Rev. Lett. **45**, 566 (1980).

[33] G. I. Csonka, J. P. Perdew, A. Ruzsinszky, P. H. T. Philipsen, S. Lebègue, J. Paier, O. A. Vydrov, and J. G. Ángyán, Phys. Rev. B **79**, 155107 (2009).

[34] J. Heyd, G. E. Scuseria, and M. Ernzerhof, J. Chem. Phys. **118**, 8207 (2003).

[35] L. Hedin, Phys. Rev. **139**, A796 (1965).

[36] M. V. Berry, Proc. R. Soc. Lond. A **392**, 45 (1984).

[37] R. D. King-Smith and D. Vanderbilt, Phys. Rev. B **47**, 1651 (1993).

[38] N. A. Spaldin, J. Solid State Chem. **195**, 2 (2012).

[39] A. Togo, F. Oba, and I. Tanaka, Phys. Rev. B **78**, 134106 (2008).

[40] A. Togo and I. Tanaka, Scr. Mater. **108**, 1 (2015).

[41] S. Baroni, S. De Gironcoli, A. Dal Corso, and P. Giannozzi, Rev. Mod. Phys. **73**, 515 (2001).

[42] D. Bucher, L. C. Pierce, J. A. McCammon, and P. R. Markwick, J. Chem. Theory Comput. **7**, 890 (2011).

[43] K. H. Michel and B. Verberck, Phys. Rev. B **83**, 115328 (2011).

[44] See Supplemental Material at http://link.aps.org/supplemental/10.1103/PhysRevB.106.054104 for more information on the structural properties of bulk h-BN, Hirshfeld-I charges, stability, in-plane Poisson's ratio, and strain-dependent band gaps for AB bilayer h-BN, which includes Refs. [61,62].

[45] R. S. Pease, Acta Crystallogr. **5**, 356 (1952).

[46] R. V. Gorbachev, I. Riaz, R. R. Nair, R. Jalil, L. Britnell, B. D. Belle, E. W. Hill, K. S. Novoselov, K. Watanabe, T. Taniguchi, A. K. Geim, and P. Blake, Small **7**, 465 (2011).

[47] S. Grimme, J. Comput. Chem. **27**, 1787 (2006).

[48] L. Li and M. Wu, ACS Nano **11**, 6382 (2017).

[49] J. J. Zhang, L. Lin, Y. Zhang, M. Wu, B. I. Yakobson, and S. Dong, J. Am. Chem. Soc. **140**, 9768 (2018).

[50] T. Aoyama, K. Yamauchi, A. Iyama, S. Picozzi, K. Shimizu, and T. Kimura, Nat. Commun. **5**, 1 (2014).

[51] T. Kimura, T. Goto, H. Shintani, K. Ishizaka, T. Arima, and Y. Tokura, Nature (London) **426**, 55 (2003).

[52] D. Khomskii, Physics **2**, 20 (2009).

[53] N. Hur, S. Park, P. A. Sharma, J. S. Ahn, S. Guha, and S. W. Cheong, Nature (London) **429**, 392 (2004).

[54] R. Jana, P. Saha, V. Pareek, A. Basu, S. Kapri, S. Bhattacharyya, and G. D. Mukherjee, Sci. Rep. **6**, 1 (2016).

[55] C. Lu and J.- M. Liu, J. Materiomics **2**, 213 (2016).

[56] G. Zhang, S. Dong, Z. Yan, Y. Guo, Q. Zhang, S. Yunoki, E. Dagotto, and J. M. Liu, Phys. Rev. B **84**, 174413 (2011).

[57] J. Beilsten-Edmands, S. J. Magorrian, F. R. Foronda, D. Prabhakaran, P. G. Radaelli, and R. D. Johnson, Phys. Rev. B **94**, 144411 (2016).

[58] G. Lawes, A. B. Harris, T. Kimura, N. Rogado, R. J. Cava, A. Aharony, O. Entin-Wohlman, T. Yildrim, M. Kenzelmann, C. Broholm, and A. P. Ramirez, Phys. Rev. Lett. **95**, 087205 (2005).

[59] K. Taniguchi, N. Abe, T. Takenobu, Y. Iwasa, and T. Arima, Phys. Rev. Lett. **97**, 097203 (2006).

[60] A. Pimenov, A. A. Mukhin, V. Y. Ivanov, V. D. Travkin, A. M. Balbashov, and A. Loidl, Nat. Phys. **2**, 97 (2006).

[61] R. C. Andrew, R. E. Mapasha, A. M. Ukpong, and N. Chetty, Phys. Rev. B **85**, 125428 (2012).

[62] F. Mouhat and F.- X. Coudert, Phys. Rev. B **90**, 224104 (2014).

[63] X. Li and J. Yang, J. Mater. Chem. C **2**, 7071 (2014).

[64] D. Lloyd, X. Liu, J. W. Christopher, L. Cantley, A. Wadehra, B. L. Kim, B. B. Goldberg, A. K. Swan, and J. S. Bunch, Nano Lett. **16**, 5836 (2016).
[65] S. Liu and R. E. Cohen, Phys. Rev. Lett. **119**, 207601 (2017).
[66] J. Kim, K. M. Rabe, and D. Vanderbilt, Phys. Rev. B **100**, 104115 (2019).
[67] P. Bultinck, C. Van Alsenoy, P. W. Ayers, and R. Carbó-Dorca, J. Chem. Phys. **126**, 144111 (2007).
[68] L. Bellaiche and D. Vanderbilt, Phys. Rev. Lett. **83**, 1347 (1999).
[69] L.-C. Zhang, G. Qin, W.-Z. Fang, H.-J. Cui, Q.-R. Zheng, Q.-B. Yan, and G. Su, Sci. Rep. **6**, 19830 (2016).
[70] S. Woo, H. C. Park, and Y.- W. Son, Phys. Rev. B **93**, 075420 (2016).
[71] G. Qin and Z. Qin, npj Comput. Mater. **6**, 1 (2020).